Differential CheR affinity for chemoreceptor C-terminal pentapeptides biases chemotactic responses

Félix Velando[#], Elizabet Monteagudo-Cascales[#], Miguel A. Matilla[*] and Tino Krell[*]

Department of Biotechnology and Environmental Protection, Estación Experimental del Zaidín, Consejo Superior de Investigaciones Científicas, Granada, Spain

Running head: CheR recognition by chemoreceptors

*Address Correspondence to Tino Krell, tino.krell@eez.csic.es, or Miguel A. Matilla miguel.matilla@eez.csic.es

# Félix Velando and Elizabet Monteagudo-Cascales contributed equally. Author order was determined by a draw.

Abstract

Chemotaxis pathways are sophisticated signal transduction systems in bacteria. Their capacity to respond to gradients of signals relies on adaptation mediated by the coordinated action of CheR methyltransferases and CheB methylesterases that control the methylation state of the signaling domain. Many chemoreceptors contain a C-terminal pentapeptide at the end of a flexible linker. In *Escherichia coli*, this pentapeptide forms a high-affinity binding site for CheR and phosphorylated CheB, and its removal interferes with adaptation. The analysis of all available chemoreceptor sequences showed that pentapeptide sequences vary greatly, and bacteria often possess multiple chemoreceptors that differ in their pentapeptide sequences. Using the phytopathogen *Pectobacterium atrosepticum*, we assessed whether this sequence variation alters CheR affinity and affects chemotaxis. The model strain SCRI1043 has 36 chemoreceptors, of which 19 possess a C-terminal pentapeptide. Using isothermal titration calorimetry, we show that the affinity of CheR for the different pentapeptides varies up to 12-fold (K_D of 86 nM to 1.04 µM). The pentapeptides with the highest and lowest affinities differed only in a single amino acid. Deletion of the *cheR* gene abolishes chemotaxis. Using quantitative immunoblot analyses, we demonstrated that the cellular CheR concentration varies during growth and is in the range of the pentapeptide affinities. PacC is the sole chemoreceptor for L-Asp in SCRI1043, and the replacement of its pentapeptide with those having the highest and lowest affinities significantly interfered with L-Asp chemotaxis. Variable C-terminal pentapeptide sequences thus provide a mechanism to bias the responses mediated by chemoreceptors.

Importance

Chemosensory pathways are notably complex. In contrast to other signal transduction mechanisms, these pathways respond to gradients rather than to constant chemical signals because of the action of adaptation enzymes. The evolutionary advantage provided by pentapeptide-containing chemoreceptors remains poorly understood. Traditionally, most chemotaxis studies analyze responses to a single compound. However, in their normal environments, bacteria are exposed to complex mixtures of chemicals that are recognized by multiple chemoreceptors. The mechanisms by which chemotactic outputs are defined in complex environments remain poorly understood. A number of features, including abundance and affinity for signals, determine the contribution of a chemoreceptor to the final response. The demonstration that the affinity of adaptation enzymes for the C-terminal pentapeptides represents another such feature provides novel insight into the processing of signals in complex environments.

Introduction

Bacterial chemotaxis is the directed swimming of bacteria in chemical gradients. It facilitates the migration of bacteria to sites that are favorable for survival. A major benefit from chemotaxis is access to nutrients (1, 2). For many human and plant pathogens with different lifestyles and infection mechanisms, chemotaxis is essential for virulence (3). Chemotaxis signaling pathways are among the most abundant prokaryotic signal transduction mechanisms (4, 5).

Chemotactic responses are typically initiated by a molecule binding to an extracytosolic sensor domain of a chemoreceptor. This binding generates a conformational change that is transmitted across the membrane to modulate the activity of the autokinase CheA, which in turn phosphorylates the CheY response regulator. Only the phosphorylated form of CheY is able to bind to the flagellar motor to control its direction and/or speed of rotation, ultimately resulting in chemotaxis (6, 7).

The capacity of chemotaxis pathways to respond to signal gradients rather than to a constant signal concentration relies on adaptation mechanisms. Canonical adaptation is based on the coordinated action of the CheR methyltransferase and the CheB methylesterase, which catalyze the methylation and demethylation, respectively, of specific glutamyl residues in the chemoreceptor signaling domain (6, 7). The importance of this adaptation mechanism is illustrated by the fact that CheR and CheB are highly conserved proteins that are present in almost all chemosensory pathways (4).

In addition to the methylation sites in the chemoreceptor signaling domain, many chemoreceptors contain an additional CheR/CheB-binding site. This consists of a C-terminal pentapeptide fused to the end of a flexible linker (8–10). Pentapeptide-containing chemoreceptors have been identified in 11 different bacterial phyla (10). Studies of *Escherichia coli* have shown that the affinity of CheR for the pentapeptide is 50 to 100-fold higher than the affinity for the methylation sites (11–13). Dissociation constants of approximately 2 µM were obtained for CheR binding to the individual pentapeptide and to the pentapeptide-containing chemoreceptor (13), indicating that all of the determinants for high-affinity CheR binding are located in the pentapeptide. In contrast to CheR, unphosphorylated CheB bound to the pentapeptide with low affinity (14–16). However, a stable phosphorylation mimic of *E. coli* CheB had a significantly higher affinity of about 13 µM, so that CheR and phosphorylated CheB both bind to the same high-affinity site (16). Partial or full truncation of the C-terminal pentapeptide from chemoreceptors greatly decreases both methylation and demethylation *in vivo* and *in vitro*, preventing chemotaxis

(12, 17–24). However, many bacteria, such as *Pseudomonas putida* KT2440, lack pentapeptide containing chemoreceptors but mediate chemotactic responses that depend on the adaptation enzymes (25–27), indicating that C-terminal pentapeptides are essential for some receptors, whereas not required for others, which corresponds to an issue that remains poorly understood.

Why are there CheR and CheB-P-binding pentapeptides at the C-terminus of chemoreceptors? It was proposed that high-affinity tethering of CheR and CheB-P to the C-terminal extension increases their local concentration, thereby enhancing their activity and leading to an optimal adaptation (16, 17, 28). In addition, we have shown previously that pentapeptides also confer specificity in their interaction with CheR and CheB in bacteria that possess multiple pathways. *Pseudomonas aeruginosa* has four chemosensory pathways, each of which contains a CheR and CheB homolog (29). Of the 26 chemoreceptors, McpB (or Aer2) is the only pentapeptide-containing chemoreceptor and the sole chemoreceptor that feeds into the Che2 pathway (30). Only $CheR_2$ and $CheB_2$, the methyltransferase and methylesterase of the Che2 pathway, but not any of the other CheR and CheB homologues bind the McpB/Aer2 pentapeptide (14, 31), permitting the targeting of a particular chemoreceptor with a specific CheR and CheB (14, 31).

All available pentapeptide sequences conserve amino acids with aromatic side chains in positions 2 and 5, whereas a significant variability is observed at the other three positions (9, 10). The inspection of the 3D structure of the CheR/pentapeptide complex of *Salmonella enterica* sv. Typhimurium shows that the aromatic side chains at positions 2 and 5 pack into two hydrophobic pockets, whereas the remaining three side chains establish hydrogen bonds and a salt bridge with CheR (32). The conservation of amino acids at positions 2 and 5 is consistent with studies showing that mutations in these positions cause severe adaptation defects (18, 22, 33, 34). Alanine-scanning mutagenesis of residues at positions 1, 3 and 4 resulted in a reduction of *in vitro* methylation and demethylation (34). Many bacterial strains contain a number of chemoreceptors that differ in their pentapeptide sequences (5), and the primary aim of this study consists in assessing how the naturally occurring variation of pentapeptide sequences within a bacterium impacts on CheR affinity and magnitude of chemotaxis.

We have addressed this question using *Pectobacterium atrosepticum* as a model. *P. atrosepticum* is among the top 10 plant pathogens (35) and is the causative agent of soft rot diseases in several agriculturally relevant crops (36). The reference strain *P. atrosepticum* SCRI1043 has 36 chemoreceptors, of which 19 possess a C-terminal

pentapeptide. We have shown previously that none of these pentapeptides are recognized by unphosphorylated or the CheB-P mimic beryllium fluoride-derivatized CheB (14). The structure of SCRI1043 CheB can be closely superimposed onto that of *Salmonella enterica* sv. Typhimurium (14, 32). SCRI1043 has a single chemosensory pathway (14), and the chemoreceptors analyzed thus far respond to amino acids (PacB, PacC), quaternary amines (PacA), and nitrate (PacN) (37–39). We show here that there are very significant differences in the affinity of the individual pentapeptides for CheR that are reflected in differences in the magnitude of the chemotactic responses. The differential recognition of CheR by pentapeptide may be a mechanism to bias chemotactic responses.

Results

SCRI1043 chemoreceptors possess 9 different pentapeptides.

A sequence alignment of the C-terminal regions of all chemoreceptors of strain SCRI1043 is shown in Fig. 1A. Nineteen chemoreceptors possess a C-terminal pentapeptide that is tethered to the signaling domain via a linker sequence of 29 to 39 amino acids (Fig. 1A). In total, there were 9 different pentapeptide sequences than can be divided into three groups (Table 1). Whereas groups 1 and 2 each contained three pentapeptides that differ in a single amino acid, group 3 contained three pentapeptides with multiple differences. All peptides possess an W and an F at positions 2 and 5, respectively, but share significant variability at the remaining positions. The NWETF pentapeptide that is found in *E. coli* and *S. enterica* sv. Typhimurium receptors is present in eight receptors (Table 1, Fig. 1A). Three pentapeptides, DWTSF, NWTTF and NWEKF, were present in two different chemoreceptors, whereas the remaining pentapeptides were found in only one chemoreceptor (Table 1, Fig. 1A). SCRI1043 chemoreceptors possess different sensor domains: PAS, sCache, Cache3_Cache2, dCache, NIT, 4HB and HBM (14). Pentapeptides are exclusively found in chemoreceptors that contain a four-helix-bundle sensor domain, either in its monomodular (4HB) or bimodular (HBM) arrangement (Table 1). Pentapeptides NWTTF and DWTSF were found in both 4HB and HBM chemoreceptors.

Conserved charge pattern in the linker/pentapeptide sequences.

So far, no conserved feature has been reported for linker sequences. They differ significantly in length, they share no apparent sequence similarities, and they are unstructured (8, 10). As expected, the alignment of the 19 linker sequences revealed no apparent sequence similarity (Fig. S1). However, there was a clear pattern of charge distribution (Fig. 1, Table S1). The N-terminal section of the linker frequently had a negative charge, followed by a central positively charged segment. The segment adjacent to the pentapeptide was negatively charged (Fig. 1, Table S1). The average calculated isoelectric point (pI) of the C-terminal 8 amino acids of these 19 linkers was 3.95 ± 0.41, whereas the calculated pI of the remaining linker was 10.82 ± 1.27 (Table S1). The plot of the electrostatic surface charge of Alphafold2 models of linker/pentapeptide segments from three representative chemoreceptors illustrates this pattern (Fig. 1B), which appears to be conserved. It is present in all pentapeptide-containing chemoreceptors from other

chemotaxis model bacteria, including *E. coli*, *S. enterica* sv. Typhimurium, *Sinorhizobium meliloti*, *Azospirillum brasilense*, *Ralstonia solanacearum*, *Comamonas testosteroni*, and *Vibrio cholerae* (Table S2).

SCRI1043 CheR binds to C-terminal pentapeptides with different affinities.

A previous study showed that SCRI1043 CheB and a CheB-P mimic failed to bind all nine C-terminal pentapeptides present in the chemoreceptors of this strain (14). To investigate whether these pentapeptides bind CheR, SCRI1043 CheR was overexpressed in *E. coli* and purified from the soluble cell lysate. To verify protein integrity, microcalorimetric titrations with S-adenosylmethionine (SAM) and S-adenosylhomocysteine (SAH), the substrate and product, respectively, of the methylation reaction, were conducted (Fig. 2). Binding of SAM and SAH was characterized by K_D values of 144 ± 22 μM and 478 ± 19 nM, respectively (Table 1), revealing that the reaction product is recognized with strong preference, which agrees with data of CheR from other species (25, 31, 40).

In subsequent studies, CheR was titrated with the nine different pentapeptides of SCRI1043. In all cases, peptides bound, but significant differences in affinity were observed (Fig. 3, Table 1). The titration with the NWETF pentapeptide (Fig. 3), present in *E. coli* and 8 SCRI1043 receptors, revealed a K_D value of 477 nM (Table 1), which is considerably higher affinity than *E. coli* CheR (K_D=2 μM) for this peptide (13). NWETF derivatives containing K and Q instead of T bound with similar affinity (Table 1). Of all peptides, GWTTF bound with highest affinity (K_D=86 nM).

Amino acid substitutions at position 1 of the pentapeptide had a pronounced effect on the binding affinity. Substitution of G by N in GWTTF resulted in the pentapeptide that bound with lowest affinity (K_D=1040 nM), representing a 12-fold reduction, whereas substitution with D caused a 2.6-fold decrease (Table 1). The three pentapeptides with three changes with respect to NWETF, namely GWQRF, GWEKF and DWTSF, bound with K_D values of 544, 197 and 361 nM, respectively (Table 1). Thus, variation in the residue at the less-conserved positions 1, 3 and 4 still significantly affects CheR binding affinity.

SCRI1043 CheR is essential for chemotaxis.

We have shown previously that SCRI1043 has multiple chemoreceptors for amino acids (38). To determine the function of CheR in SCRI1043, we constructed a *cheR*

deletion mutant. Quantitative chemotaxis capillary assays showed that this mutant is unable to perform chemotaxis to casamino acids or L-aspartate. Many bacteria are strongly attracted by Krebs cycle intermediates (41). We observed a strong attraction of SCRI1043 to L-malate, for which the corresponding chemoreceptor(s) remain(s) unknown (Fig. 4). The *cheR* mutant also failed to be attracted to L-malate, indicating that CheR is essential to perform chemotaxis toward amino acids and at least one organic acid.

The concentration of intracellular CheR is similar to CheR-pentapeptide affinities

Having determined the K_D values for the CheR-pentapeptide interactions, we hypothesized that a differential occupation of chemoreceptor pentapeptides because of different affinities can alter the magnitude of chemotaxis. However, to assess the physiological relevance of differential pentapeptide binding, the concentration of intracellular CheR must be known. A further question is whether the CheR concentration changes with the growth phase. We thus determined the intracellular CheR concentration during the exponential and stationary growth phases by quantitative immunoblotting.

CheR polyclonal antibodies were generated by rabbit immunization (see Materials and Methods). Immunoblotting of the wild-type (wt) and the Δ*cheR* mutant strains demonstrated the specificity of CheR-antibody interaction (Fig. 5). For the SCRI1043 samples used in immunoblots, the cell number was determined by plating out serial dilutions. Using this cell number and the cell volume as derived from electron microscopy, the intracellular CheR concentrations in exponential and stationary phase cultures were determined to be 1.4 ± 0.3 μM and 0.73 ± 0.1 μM, respectively. These data show that: (1) the cellular CheR concentration is within the range of K_D values for pentapeptide binding; and (2) that the CheR concentration in stationary phase is about half what it is during growth.

Alteration of PacC mediated chemotaxis by substitution of pentapeptides

A previous study demonstrated that the strong chemotactic response of SCRI1043 to L-Asp depends entirely on the PacC chemoreceptor (38). As in *E. coli* Tar, PacC is encoded in the chemosensory signaling cluster and contains the NWETF pentapeptide. As shown above, CheR recognizes this pentapeptide with a K_D of 477 nM. To investigate the relevance of the CheR affinity for the pentapeptide in the chemotactic response to L-Asp, we generated two chromosomal mutations in which the region encoding the original pentapeptide was altered to encode GWTTF or NWTTF, which bind CheR with either

the highest (K_D=86 nM) or lowest (K_D=1040 nM) affinity, respectively. Control capillary chemotaxis assays showed that the responses of wt and mutant strains to casamino acids are indistinguishable (Fig. S2).

Chemotaxis experiments with the wt strain showed strong responses towards different L-Asp concentrations, confirming previously published data (38). When these experiments were repeated with the mutant strain encoding PacC containing the NWTTF pentapeptide (lowest affinity), a statistically significant drop in the chemotaxis magnitude was observed at concentrations of 0.1 to 10 mM L-Asp (Fig. 6). Notably, a similar reduction was observed when the assays were made with the mutant strain encoding PacC-GWTTF (highest affinity) (Fig. 6). These data demonstrate that the affinity of the CheR-pentapeptide interaction influences the chemotactic response. Either tighter or looser binding of CheR was associated with a decreased chemotaxis response to L-Asp.

Discussion

E. coli and *S. enterica* sv. Typhimurium are the traditional model organisms in chemotaxis research. Two of their chemoreceptors, Tar and Tsr, contain the NWETF pentapeptide and most of what we know about pentapeptide function is therefore based on the study of the NWETF (11–13, 24, 32–34, 42, 43). Bioinformatic studies of all available chemoreceptor sequences show that their C-terminal pentapeptides differ in sequence (9, 10), and many strains contain receptors with pentapeptides having different sequences (5). Here, we present the first study evaluating CheR recognition of the complete set of different pentapeptides within a bacterial strain.

A previous study showed that native CheB or the beryllium fluoride-modified CheB-P mimic of SCRI1043 did not interact with any of these pentapeptides (14), although it is unknown if an interaction with CheB-P may occur *in vivo*. In contrast, all 9 pentapeptides were recognized by SCRI1043 CheR. The affinities were between 86 nM and 1.04 µM, and thus higher than the affinity of *E. coli* CheR for NWETF of about 2 µM (11, 13), but comparable to the K_D of about 500 nM derived for the interaction of *P. aeruginosa* $CheR_2$ with the GWEEF peptide of the McpB/Aer2 chemoreceptor (31).

The importance of each of the 5 amino acids of the NWETF pentapeptide in *E. coli* has been investigated using alanine-scanning mutagenesis (34). Whereas mutation of W and F abolished methylation and demethylation *in vitro*, mutations of the remaining three amino acids resulted in a partial reduction of both activities. However, alanine is an amino acid that is rarely found in positions 1, 3 and 4 (9, 10). Here, we investigated naturally occurring pentapeptides and found that they differ in their affinity for CheR by up to 12-fold. These alterations are consistent with the 3D structure of the *S. enterica* CheR/pentapeptide complex showing that the N and T of the NWETF pentapeptide establish hydrogen bonds with the protein, whereas the E forms a salt bridge with a CheR Arg residue (32). Altering these interactions by amino acid replacements might be expected to alter binding affinity.

The notion that residues at positions 1, 3, and 4 do not occur in a random fashion but are rather the result of evolution is supported by several observations. First, the sequence logo of all naturally occurring pentapeptides shows clear amino acid preference. In all three positions aspartate or glutamate residues are predominant (10). Second, the single amino acid substitutions in pentapeptides of groups 1 and 2 are frequently caused by two nucleotide changes (Table 1) and are thus not single nucleotide polymorphisms.

In their natural environment, bacteria are exposed to complex mixtures of compounds, many of which are chemoeffectors. Also, in many bacteria, multiple chemoreceptors stimulate a single chemotaxis pathway (5). However, the mechanisms that permit the generation of specific chemotactic responses in the presence of complex chemoeffector mixtures is unclear.

How is the weight an individual chemoreceptor in the final response determined? One contribution is the affinity with which individual chemoeffectors are recognized by different chemoreceptors; a parameter that is known to determine the onset of a chemotactic response (10, 44). Other factors are the level of expression and cellular abundance of chemoreceptors (45, 46). Here, we have found that changes in the pentapeptide sequence can also alter the magnitude of the chemotactic response. We show that the intracellular CheR concentration is in the range of the K_D values of the pentapeptide for binding CheR. Thus, receptors with different pentapeptide sequences will be differentially occupied with CheR. In contrast to *E. coli*, where CheB was found to bind to the pentapeptide (16), we have failed to observe an interaction of any of the pentapeptides the *P. atrosepticum* CheB either in its unphosphorylated form or as a CheB-P mimic (14). However, an interaction with CheB-P may occur in the cell, and the failure to detect this interaction *in vitro* may be due to a technical issue. Considering that pentapeptides differ in their affinities for CheR, it is reasonable to suggest that such differences may also occur for binding of CheB-P. Thus, an altered interaction with CheB-P may also contribute to the dependence of PacC-mediated aspartate taxis seen with different pentapeptide sequences.

Optimal chemotaxis to L-Asp was observed when the PacC receptor contained its native NWETF pentapeptide, which has a mean K_D for CheR of 477 nM. When the pentapeptide was converted to NWTTF, which binds CheR with a K_D that is ~2.2-fold higher (1.04 µM), or to GWTTF, which binds CheR with a K_D that is ~5.5-fold lower (86 nM), the chemotactic responses were lower. This effect was a 2.1-fold for NWTTF or 1.6 fold for GWTTF when the aspartate concentration in the capillaries was 1 mM, and 1.4-fold or 1.5-fold for NWTTF or GWTTF, respectively, when the aspartate concentration was 10 mM. These differences are modest but statistically significant. As noted above, the affinity of different pentapeptides for the other adaptation enzyme, the CheB-P demethylase, may also vary. In any case, it is clear that the extent of chemoreceptor occupation by adaptation enzymes is finely tuned to achieve optimum chemotaxis.

CheR and CheB-P tethered at the C-terminal pentapeptide act not only on its cognate chemoreceptors, but also on neighboring receptors (28, 47). We show here that the alteration of the pentapeptide sequence did not modulate chemotaxis to amino acids (Fig. S2). SCRI 1043 chemotaxis to amino acids is mediated by three chemoreceptors, namely PacA, PacB and PacC (38). Of these, only PacC has a C-terminal pentapeptide. These data suggest that CheR recognition by the pentapeptide impacts primarily the activity of the cognate receptor. However, future studies will be required to explore this issue in a comprehensive manner.

The linker that leads to the pentapeptide does not have a conserved sequence. It is considered to be an unstructured, disordered and flexible arm that facilitates the movement of tethered adaptation enzymes within the receptor array (8). We report here that there is a conserved distribution of charge within SCRI1043 chemoreceptors (Table S1) that is also conserved in the receptors of bacteria that belong to different phylogenetic categories (Table S2). This pattern is independent of linker length: it was detected in the 29-residue linker of the *S. enterica* sv. Typhimurium Tcp chemoreceptor as well as in the 91-residue linker of *R. solanacearum* RS_RS23910 (Table S2). Our observations should prompt studies to investigate the functional relevance of this pattern. The signaling domain of chemoreceptors typically has a significant negative surface charge (48) (Fig. S3). The positive charge of the central linker segment may mediate a charge attraction with the signaling domain, whereas the negative charge of the C-terminal portion of the linker that connects to the pentapeptide may cause a repulsion away from the signaling domain. The notion that this conserved charge pattern is of functional relevance is supported by a study of *E. coli* Tar (24). The authors generated alanine-substitution mutants of the lysine and three arginine residues present in the Tar linker (Table S2). Whereas receptors with individual substitutions supported chemotaxis equivalent to that supported by wild-type Tar, combining all four changes decreased chemotaxis by about 50%. Importantly, the singly substituted receptors showed a significant increase in CheA activity that was increased when multiple substitutions were combined. The authors concluded that the Ala substitutions either stabilize the ON state or destabilize the OFF state. Whereas the initial 30 amino acids of this linker have a calculated pI of 10.74 (Table S2), replacing all four positively charged amino acids with Ala lowered the pI to 3.80. It was suggested that the positively charged linker either interacts with the negatively charged polar head groups of phospholipids or with charged residues in the signaling domain of the receptor (24). Combined with the observation that this charge pattern is

conserved, this result supports the idea that this organization of the linker is of fundamental functional relevance.

Collectively, we show here that naturally occurring variations in the pentapeptide sequence cause important alterations in the binding affinities of CheR and possibly also for CheB-P. These variations in the recognition of adaptation enzymes are reflected in the magnitude of chemotaxis. Maximal responses were obtained for a chemoreceptor containing its naturally occurring pentapeptide, suggesting that the pentapeptide sequence has been fine-tuned to guarantee maximal responses. A conserved charge pattern was observed in linker sequences that is likely to contribute to the spatial organization of the linker within the chemoreceptor array. Our study forms the basis for investigations on how pentapeptide sequence variation affects the magnitude of chemotaxis in other bacteria and to determine the functional relevance of the observed charge pattern of the linker.

Materials and Methods

Bacterial strains and growth conditions: Bacterial strains used in this study are listed in Table S3. SCRI1043 and its derivative strains were routinely grown at 30 °C in Luria Broth (5 g/l yeast extract, 10 g/l bacto tryptone, 5 g/l NaCl) or minimal medium (0.41 mM $MgSO_4$, 7.56 mM $(NH_4)_2SO_4$, 40 mM K_2HPO_4, 15 mM KH_2PO_4) supplemented with 0.2% (w/v) glucose as carbon source. *E. coli* strains were grown at 37 °C in LB. *Escherichia coli* DH5α was used as a host for gene cloning. Media for propagation of *E. coli* β2163 were supplemented with 300 mM 2,6-diaminopimelic acid. When appropriate, antibiotics were used at the following final concentrations (in μg ml^{-1}): kanamycin, 50; streptomycin, 50; ampicillin, 100. Sucrose was added to a final concentration of 10% (w/v) when required to select derivatives that had undergone a second cross-over event during marker exchange mutagenesis.

In vitro nucleic acid techniques: Plasmid DNA was isolated using the NZY-Tech miniprep kit. For DNA digestion, the manufacturer's instructions were followed (New England Biolabs and Roche). Separated DNA fragments were recovered from agarose using the Qiagen gel extraction kit. Ligation reactions were performed as described in (49). PCR reactions were purified using the Qiagen PCR Clean-up kit. PCR fragments were verified by DNA sequencing that was carried out at the Institute of Parasitology and Biomedicine Lopez-Neyra (CSIC; Granada, Spain). Phusion® high fidelity DNA polymerase (Thermo Fisher Scientific) was used in the amplification of PCR fragments for cloning.

CheR overexpression and purification: The DNA sequence encoding CheR of SCRI1043 (ECA_RS08375) was amplified by PCR using the oligonucleotides indicated in Table S4 and genomic DNA as template. The PCR product was digested with NheI and SalI and cloned into pET28b(+) linearized with the same enzymes. The resulting plasmid pET28b-CheR was verified by DNA sequencing and transformed into *E. coli* BL21-AI™. The strain was grown under continuous stirring (200 rpm) at 30 ºC in 2-liter Erlenmeyer flasks containing 500 ml of LB medium supplemented with 50 μg/ml kanamycin. At an OD_{660} of 0.6, protein expression was induced by the addition of 0.1 mM isopropyl β-D-1-thiogalactopyranoside (IPTG) and 0.2 % (w/v) L-arabinose. Growth was continued at 16 °C overnight prior to cell harvest by centrifugation at 10 000 x *g* for 30 min. The cell

pellet was resuspended in buffer A (40 mM KH_2PO_4/K_2HPO_4, 10 mM imidazole, 10% (v/v) glycerol, 1 mM β-mercaptoethanol, pH 7.5) and cells were broken by French press treatment at 62.5 lb/in^2. After centrifugation at 20 000 x *g* for 30 min, the supernatant was loaded onto a 5-ml HisTrap HP columns (Amersham Biosciences) equilibrated with buffer A and eluted with an imidazole gradient of 40–500 mM in the same buffer. Protein-containing fractions were pooled, and dialyzed overnight against 40 mM KH_2PO_4/K_2HPO_4, 10% (v/v) glycerol, 1 mM β-mercaptoethanol, pH 7.0. For the purification of CheR that was used for animal immunization or as standard in the immunoblot, protein was further purified by size exclusion chromatography on a HiPrepTM 26/60 SephacrylTM S200 HR gel filtration column (GE Healthcare). Protein was eluted isocratically at a flow of 1 ml/min. All manipulations were carried out at 4 ºC.

Isothermal titration calorimetry (ITC): All experiments were conducted on a VP-microcalorimeter (MicroCal, Amherst, MA) at 25 °C. CheR was dialyzed overnight against 40 mM KH_2PO_4/K_2HPO_4, 10% (v/v) glycerol, 1 mM β-mercaptoethanol, pH 7.0, adjusted to a concentration of 10–20 μM, placed into the sample cell and titrated with 3.2–4.8 μl aliquots of 0.1–1 mM peptide solutions (purchased from GenScript, Piscataway, NJ, USA), 2 mM SAM or 250 μM SAH. All solutions were prepared in dialysis buffer immediately before use. The mean enthalpies measured from the injection of the peptide into the buffer were subtracted from raw titration data prior to data analysis with the MicroCal version of ORIGIN. Data were fitted with the 'One binding site model' of ORIGIN.

Construction of a mutant deficient in cheR. A chromosomal *cheR* mutant of SCRI1043 was constructed by homologous recombination using a derivative plasmid of the suicide vector pKNG101. The up- and downstream flanking regions of *cheR* were amplified by PCR using the oligonucleotides listed in Table S4, which were subsequently digested with EcoRI/BamHI and BamHI/PstI, respectively, and ligated in a three-way ligation into the EcoRI/PstI sites of pUC18Not to generate pUC18Not_ΔcheR. Subsequently, a 0.95-kb BamHI fragment containing the Km3 cassette of p34S-Km3 was inserted into the BamHI site of pUC18Not_ΔcheR, giving rise to pUC18Not_ΔcheR_km3. Lastly, a ~2.5-kb NotI fragment of pUC18Not_ΔcheR_km3 was cloned at the same site into pKNG101, resulting in pKNG101_ΔcheR. This plasmid was transferred to SCRI1043 by biparental conjugation using *E. coli* β2163. Then, cells were spread onto LB plates containing

kanamycin at 50 µg/ml. Selected merodiploid colonies were spread onto LB plates containing 10 % (w/v) sucrose to select derivatives that had undergone a second cross-over event during marker exchange mutagenesis. All plasmids and the final mutant were confirmed by PCR and sequencing.

Construction of SCRI1043 mutant strains pacC-*NWTTF and* pacC-*GWTTF*. Chromosomal mutants of SCRI1043 encoding PacC variants with altered pentapeptides were constructed by homologous recombination using derivative plasmids of the suicide vector pKNG101. Briefly, an overlapping PCR mutagenesis approach was employed to construct *pacC* gene variants in which the region encoding the original NWETF pentapeptide sequence was altered to encode GWTTF or NWTTF, using oligonucleotides listed in Table S4. The corresponding ~1-kb PCR products were then digested with EcoRI/PstI and cloned into the same sites of pUC18Not to generate pUC18Not-pacC-NWTTF and pUC18Not-pacC-GWTTF. Subsequently, ~1.1-kb NotI fragments of these plasmids were cloned at the same site in pKNG101 to generate pKNG-pacC-NWTTF and pKNG-pacC-GWTTF, which were transferred to *P. atrosepticum* SCRI1043 by biparental conjugation using *E. coli* β2163. After overnight incubation at 30 ºC, cells were spread onto LB plates containing streptomycin at 50 µg/ml. Selected merodiploid colonies were spread onto LB plates containing 10 % (w/v) sucrose to select derivatives that had undergone a second cross-over event during marker exchange mutagenesis. All plasmids and final mutants were confirmed by PCR and sequencing.

Quantitative capillarity chemotaxis assays. Overnight bacterial cultures of SCRI1043 were grown at 30 ºC in minimal medium. At an OD_{660} of 0.3-0.4, the cultures were washed twice by centrifugation (1,667 × *g* for 5 min at room temperature) and subsequent resuspension in chemotaxis buffer (50 mM K_2HPO_4/KH_2PO_4, 20 µM EDTA and 0.05% (v/v) glycerol, pH 7.0). Cells were diluted to an OD_{660} of 0.1 in the same buffer. Subsequently, 230 µl aliquots of the resulting bacterial suspension were place into 96-well plates. One-microliter capillary tubes (P1424, Microcaps; Drummond Scientific) were heat-sealed at one end and filled with either the chemotaxis buffer (negative control) or chemotaxis buffer containing the chemoeffectors to test. The capillaries were immersed into the bacterial suspensions at its open end. After 30 min at room temperature, the capillaries were removed from the bacterial suspensions, rinsed with sterile water and the content expelled into tubes containing 1 ml of minimal medium salts. Serial dilutions

were plated onto minimal medium supplemented with 15 mM glucose as carbon source. The number of colony forming units was determined after 36 h incubation at 30 ºC. In all cases, data were corrected with the number of cells that swam into buffer containing capillaries. Data are the means and standard deviations from at least three biological replicates conducted in triplicate.

Determination of the cellular CheR concentration by quantitative immunoblotting. Generation of the acetone powder: Sera of polyclonal antibodies were obtained from Biotech Corp (Piscataway, New Jersey, USA) by an immunization of rabbit with highly purified CheR. The specificity of the CheR-antibody interaction was optimized by preincubation of the antiserum with a cytoplasmic extract from the Δ*cheR* mutant (or acetone powder). To this end an acetone powder pre-absorption protocol similar to that described in (50) was used. To this end a 700 ml culture of SCRI1043 Δ*cheR* was grown in minimal medium supplemented with 15 mM glucose until an OD_{660} of 0.8 and cells were harvested by centrifugation at 10 000 x *g* for 10 minutes (4 ºC). Cells were then resuspended in 4 ml of 0.9% NaCl (w/v) to which 16 ml acetone were added. After an incubation for 30 minutes, the sample was centrifuged at 10 000 x *g* for 10 minutes, the pellet resuspended in 20 ml acetone and kept on ice for 10 minutes. This solution was centrifuged as above and the pellet was dried and homogenized to a powder, prior to storage at -20 ºC. The antibody solution was diluted three-fold with phosphate buffer saline (PBS), prior to the addition of this acetone powder to a final concentration of 1% (w/v). This suspension was incubated at room temperature for 30 minutes and then centrifuged at 13 000 x *g* for 5 min. The supernatant was recovered and then diluted 200-fold with PBS to be used in the immunoblots as detailed below.

Cell culture and western blot analysis: The wt and Δ*cheR* strains were grown in minimal medium as detailed above. Twenty ml samples were taken during exponential phase (OD_{660}=0.5) or late stationary phase (overnight culture with OD_{660}>2.5) and cells harvested by centrifugation at 10 000 x *g* during 5 min. In parallel, the number of cells in both samples was determined by plating out serial dilutions and cell counting. Cell pellets were resuspended in buffer A (40 mM K_2HPO_4/KH_2PO_4, 10 mM imidazole, 10 % (v/v) glycerol, 1 mM β-mercaptoethanol, pH 7.0) containing the cOmplete^{TM} EDTA-Free protease inhibitor at a 1 x concentration following manufacturer´s instructions (Merck Millipore, Darmstadt, Germany). The buffer volume was proportional to the cell density of the sample. This buffer was identified in buffer screening experiments with purified

CheR and was found to maintain the protein stable and active. Cells were sonicated and Benzonase® Nuclease (Merck, Millipore Corp, Burlington, Massachusetts, USA) was added at a concentration of 1 U/ml. After an incubation at 25 ºC during 10 minutes, samples were adjusted to the same protein concentration prior to the addition of SDS sample buffer. Samples were incubated at 95 ºC for 10 minutes and, along with 1 to 10 ng aliquots of purified CheR, separated on 12 % (w/v) SDS-PAGE gels. SDS-PAGE electrophoresis was done at 120 V, prior to protein transfer onto 0.45 µm-pore-size nitrocellulose membranes (Protram Premium; Amersham Pharmacia Biotech, Amersham, UK) at 100 V for 1-2 h. Nitrocellulose membranes were immersed in 10% (w/v) nonfat powdered milk in PBS and placed on an orbital shaker at 4 ºC for 12 h. Subsequently, membranes were immersed in a 1/200 dilution of primary antiserum in PBS + 10 % (w/v) milk, placed on an orbital shaker at room temperature for 2 h. Membranes were then washed three times with PBS for 10 min, incubated with a 1/5000 dilution of secondary Goat anti-Rabbit IgG (H+L) (Thermofisher Scientific, Waltham, Massachusetts, USA) for 1-2 h, washed as above, and treated with Femto ECL Western blotting detection reagent (Amersham Pharmacia Biotech, Amersham, UK) according to the manufacturer's protocol and exposed to a chemiluminescent detector (Bio-Rad ChemiDoc™ XRS+ System, Bio-Rad, Hercules, California, USA). Chemiluminescent images were captured, and intensities were quantified using Quantity One software (Bio-Rad, Hercules, California, USA).

Calculation of the cellular CheR concentration: The amount of CheR present in samples was inferred from the standard curve (Fig. S4). The determination of the cellular CheR concentration was based on the normalization of absolute values with the number of cells and the cell volume. The SCRI1043 cell volume was derived from electron microscopy studies. To this end cells were cultured as detailed above and fixed with a solution of 2.5 % (v/v) glutaraldehyde containing 100 mM sodium cacodylate. Subsequently a 0.1 % (w/v) solution of poly-L-Lys in water was deposited on a coverslip to which the fixed sample was added. An aqueous solution of 1% (w/v) osmium tetroxide was then applied to the sample and incubated at 4 ºC for 1 hour. The coverslip was then washed with distillated water and the sample was dehydrated by applying an ethanol gradient (50 %, 70 %, 90 % and 3 x 100 %), with 10 minutes per step. Finally, the samples were dried by the Critical Point Method (51) in a desiccator Polaron CPD 7501. Finally, cells are covered with a carbon sheet (EMITECH K975X). Images were recorded using a Scanning Electron Microscope HITACHI S-510. From the resulting images, the length

and width of 200 individual, non-attached cells (Fig. S5) were determined using the ImageJ software (U. S. National Institutes of Health, Bethesda, Maryland, USA). The cell volume was calculated by approximating the shape of cells to a spherocylinder, i.e. a cylinder with hemispherical caps, using $V = \pi R^2 (L - 2R) + 4/3\pi R^3 = \pi R^2 (L - 2/3R)$ (52) where V= volume; R=radius and L=length. Cell volumes of $0.71 \pm 0.04\ \mu m^3$ and $0.82 \pm 0.02\ \mu m^3$ for cells in the exponential and stationary phases, respectively sere determined. Cellular CheR concentrations are the means and standard errors of three biological replicates conducted in duplicates.

Acknowledgements: We are indebted to Dr. Michael Manson for his constructive scientific criticism and editing the English of this manuscript. We would also like to thank Dr. Gerald Hazelbauer for his advice in preparing the acetone powder. This work was supported by the Spanish Ministry for Science and Innovation/*Agencia Estatal de Investigación* 10.13039/501100011033 through grants PID2020-112612GB-I00 to TK and PID2019-103972GA-I00 to MAM, CSIC grant 2023AEP002 to MAM, and the Junta de Andalucía (grant P18-FR-1621 to TK).

Abbreviations: 4HB, four-helix bundle domain; HBM, helical bimodular domain; ITC, isothermal titration calorimetry; LBD, ligand binding domain; SCRI1043, *Pectobacterium atrosepticum* SCRI1043; SAM, S-adenosylmethionine; SAH, S-adenosylhomocysteine.

Figure legends

Fig. 1) C-terminal pentapeptides at *P. atrosepticum* SCRI1043 chemoreceptors. A) The C-terminal section of the sequence alignment of SCRI1043 chemoreceptors is shown. Pentapeptides are shaded in grey. The linker sequences are underlined. Green: conserved residues in the signaling domain; red: Asp and Glu; blue: Lys and Arg. B) The electrostatic surface potential of the linker + pentapeptide sequences from three representative SCRI1043 chemoreceptors. Fragments from molecular models of the entire receptor generated by Alphafold2 (53) are shown. Calculations were made using the "APBS Electrostatics" plugin of PyMOL (54). Blue: positive charge; red: negative charge.

Fig. 2) Binding of S-adenosylmethionine (SAM) and S-adenosylhomocysteine (SAH) to *P. atrosepticum* CheR. Microcalorimetric titrations of 10 µM CheR with 16 µl aliquots of 2 mM SAM (A) and of 14 µM CheR with 4.8 µl aliquots of 250 µM SAH (B). Upper panel: Raw titration data. Lower panel: Data corrected for dilution heat and concentration-normalized integrated peak areas of raw titration data. Data were fitted with the "One binding site model" of the MicroCal version of ORIGIN.

Fig. 3) Interaction between *P. atrosepticum* pentapeptides and CheR. Upper panel: Microcalorimetric titrations of 16-20 µM CheR with 1 mM solutions of pentapeptides NWTTF, NWETF and GWTTF. Lower panel: Data corrected for dilution heat and concentration-normalized integrated peak areas of raw titration data. Data were fitted with the "One binding site model" of the MicroCal version of ORIGIN. Derived binding parameters are provided in Table 1.

Fig. 4) Quantitative capillary chemotaxis assays of wild-type *P. atrosepticum* SCRI1043 and a Δ*cheR* mutant towards different chemoattractants. Data have been corrected for the number of cells that swam into buffer containing capillaries (113 ± 19, 370 ± 64, and 305 ± 49 cells/capillary for L-malate, casamino acids (CAA), and L-aspartate, respectively). The means and standard deviations from three independent experiments conducted in triplicate are shown.

Fig. 5) Immunoblot of *P. atrosepticum* SCRI1043 samples and purified CheR using polyclonal antibodies against CheR. Lanes 1 and 2: two dilutions of SCRI1043 Δ*cheR*; lanes 3 and 4: two dilutions of SCRI1043 (wt); M: molecular weight marker. The remaining four lanes contain different amounts purified SCRI1043 CheR.

Fig. 6) Quantitative L-Asp capillary chemotaxis assays of wild type *P. atrosepticum* SCRI1043 and chromosomal mutants containing variations in the PacC pentapeptide sequence. Data have been corrected for the number of bacteria that swam into buffer-containing capillaries (872 ± 271 for wt, 879 ± 167 for the PacC-NWTTF mutant, and 445 ± 117 for the PacC-GWTTF mutant). Data are the means and standard deviations from at least three biological replicates conducted in triplicate. * $P<0.05$; ** $P<0.01$ (Student's t-test).

Table 1) Binding parameters for the interaction of *P. atrosepticum* CheR with S-adenosylmethionine (SAM), S-adenosylhomocysteine (SAH) and pentapeptides. Amino acid changes and the corresponding alterations in the nucleotide sequence in pentapeptides from groups 1, 2 and 3 with respect to the reference pentapeptide in each group are highlighted in red color.

Pentapeptide group[a]	Ligand	Nucleotide sequence in corresponding gene	Chemoreceptor (sensor domain type)[b]	K_D[c]	ΔH (kcal/mol)
-	SAM	-	-	144 ± 22 µM	-15.1 ± 3
	SAH	-	-	478 ± 19 nM	-17.7 ± 0.3
Group 1	NWETF	AACTGGGAAACCTTT	ECA_RS21450 (4HB)	477 ± 37 nM	-11.5 ± 2
		AACTGGGAAACCTTT	ECA_RS21455 (4HB)		
		AATTGGGAAACCTTC	ECA_RS08370 (4HB)		
		AATTGGGAAACGTTT	ECA_RS06345 (4HB)		
		AACTGGGAAACGTTC	ECA_RS08330 (4HB)		
		AATTGGGAAACGTTC	ECA_RS19280 (4HB)		
		AACTGGGAAACTTTC	ECA_RS13300 (4HB)		
		AACTGGGAAACCTTT	ECA_RS21445 (4HB)		
	NWEKF	AACTGGGAAAAATTC	ECA_RS20365 (4HB)	788 ± 154 nM	-12.1 ± 0.5
		AACTGGGAAAAATTC	ECA_RS06625 (4HB)		
	NWEQF	AACTGGGAACAGTTC	ECA_RS21440 (4HB)	433 ± 23 nM	-16.0 ± 2
Group 2	NWTTF	AATTGGACGACGTTC	ECA_RS00900 (4HB)	1.04 ± 0.23 µM	-12.0 ± 1
		AACTGGACAACGTTC	ECA_RS00400 (HBM)		
	GWTTF	GGCTGGACGACATTC	ECA_RS12635 (HBM)	86 ± 9 nM	-16.7 ± 2.5
	DWTTF	GACTGGACCACGTTC	ECA_RS08780 (4HB)	226 ± 39 nM	-12.9 ± 1
Group 3	GWQRF	GGCTGGCAGCGTTTT	ECA_RS15955 (4HB)	544 ± 107 nM	-9.8 ± 0.2
	GWEKF	GGATGGGAAAAGTTC	ECA_RS07510 (4HB)	197 ± 38 nM	-12.5 ± 1
	DWTSF	GACTGGACATCGTTC	ECA_RS18000 (4HB)	361 ± 61 nM	-10.7 ± 1
		GACTGGACGTCGTTT	ECA_RS12640 (HBM)		

[a]The pentapeptides were classified into 3 groups depending on the number of changes in the amino acid residues with respect to the reference pentapeptide in the group, with groups 1 and 2 presenting one change, whereas pentapeptides in group 3 present two or three amino acid changes. Residues that differ from NWETF (group 1), NWTTF (group 2) or GWQRF (group 3) are shown in red font.
[b]4HB: 4-helix bundle domain; HBM: helical bimodular domain.
[c]Data were derived from microcalorimetric titrations (Fig. 3).

References

1. Colin R, Ni B, Laganenka L, Sourjik V. 2021. Multiple functions of flagellar motility and chemotaxis in bacterial physiology. FEMS Microbiol Rev, 2021/07/07 ed. 45:fuab038.
2. Matilla MA, Gavira JA, Krell T. 2023. Accessing nutrients as the primary benefit arising from chemotaxis. Curr Opin Microbiol 75:102358.
3. Matilla MA, Krell T. 2018. The effect of bacterial chemotaxis on host infection and pathogenicity. FEMS Microbiol Rev 42:fux052.
4. Wuichet K, Zhulin IB. 2010. Origins and diversification of a complex signal transduction system in prokaryotes. Sci Signal 3:ra50.
5. Gumerov VM, Ulrich LE, Zhulin IB. 2023. MiST 4.0: a new release of the microbial signal transduction database, now with a metagenomic component. Nucleic Acids Res gkad847.
6. Parkinson JS, Hazelbauer GL, Falke JJ. 2015. Signaling and sensory adaptation in Escherichia coli chemoreceptors: 2015 update. Trends Microbiol 23:257–66.
7. Bi S, Sourjik V. 2018. Stimulus sensing and signal processing in bacterial chemotaxis. Curr Opin Microbiol 45:22–29.
8. Bartelli NL, Hazelbauer GL. 2011. Direct evidence that the carboxyl-terminal sequence of a bacterial chemoreceptor is an unstructured linker and enzyme tether. Protein Sci 20:1856–66.
9. Perez E, Stock AM. 2007. Characterization of the Thermotoga maritima chemotaxis methylation system that lacks pentapeptide-dependent methyltransferase CheR:MCP tethering. Mol Microbiol 63:363–78.
10. Ortega Á, Krell T. 2020. Chemoreceptors with C-terminal pentapeptides for CheR and CheB binding are abundant in bacteria that maintain host interactions. Comput Struct Biotechnol J 18:1947–1955.
11. Li M, Hazelbauer GL. 2020. Methyltransferase CheR binds to its chemoreceptor substrates independent of their signaling conformation yet modifies them differentially. Protein Sci 29:443–454.
12. Barnakov AN, Barnakova LA, Hazelbauer GL. 1999. Efficient adaptational demethylation of chemoreceptors requires the same enzyme-docking site as efficient methylation. Proc Natl Acad Sci U S A 96:10667–72.

13. Wu J, Li J, Li G, Long DG, Weis RM. 1996. The receptor binding site for the methyltransferase of bacterial chemotaxis is distinct from the sites of methylation. Biochemistry 35:4984–93.
14. Velando F, Gavira JA, Rico-Jimenez M, Matilla MA, Krell T. 2020. Evidence for Pentapeptide-Dependent and Independent CheB Methylesterases. Int J Mol Sci 21:E8459.
15. Barnakov AN, Barnakova LA, Hazelbauer GL. 2002. Allosteric enhancement of adaptational demethylation by a carboxyl-terminal sequence on chemoreceptors. J Biol Chem 277:42151–6.
16. Li M, Xu X, Zou X, Hazelbauer GL. 2021. A Selective Tether Recruits Activated Response Regulator CheB to Its Chemoreceptor Substrate. mBio 12:e0310621.
17. Le Moual H, Quang T, Koshland DE Jr. 1997. Methylation of the Escherichia coli chemotaxis receptors: intra- and interdimer mechanisms. Biochemistry 36:13441–8.
18. Okumura H, Nishiyama S, Sasaki A, Homma M, Kawagishi I. 1998. Chemotactic adaptation is altered by changes in the carboxy-terminal sequence conserved among the major methyl-accepting chemoreceptors. J Bacteriol 180:1862–8.
19. Li J, Li G, Weis RM. 1997. The serine chemoreceptor from Escherichia coli is methylated through an inter-dimer process. Biochemistry 36:11851–7.
20. Li M, Hazelbauer GL. 2006. The carboxyl-terminal linker is important for chemoreceptor function. Mol Microbiol 60:469–79.
21. Russo AF, Koshland DE. 1983. Separation of signal transduction and adaptation functions of the aspartate receptor in bacterial sensing. Science 220:1016–1020.
22. Yamamoto K, Imae Y. 1993. Cloning and characterization of the Salmonella typhimurium-specific chemoreceptor Tcp for taxis to citrate and from phenol. Proc the Natl Acad Sci USA 90:217–21.
23. Uchida Y, Hamamoto T, Che Y-S, Takahashi H, Parkinson JS, Ishijima A, Fukuoka H. 2022. The Chemoreceptor Sensory Adaptation System Produces Coordinated Reversals of the Flagellar Motors on an Escherichia coli Cell. J Bacteriol 204:e0027822.
24. Lai R-Z, Bormans AF, Draheim RR, Wright GA, Manson MD. 2008. The region preceding the C-terminal NWETF pentapeptide modulates baseline activity and aspartate inhibition of Escherichia coli Tar. Biochemistry 47:13287–13295.

25. García-Fontana C, Reyes-Darias JA, Muñoz-Martínez F, Alfonso C, Morel B, Ramos JL, Krell T. 2013. High specificity in CheR methyltransferase function: CheR2 of Pseudomonas putida is essential for chemotaxis, whereas CheR1 is involved in biofilm formation. J Biol Chem 288:18987–18999.
26. García V, Reyes-Darias J-A, Martín-Mora D, Morel B, Matilla MA, Krell T. 2015. Identification of a Chemoreceptor for C2 and C3 Carboxylic Acids. Appl Environ Microbiol 81:5449–5457.
27. Martín-Mora D, Reyes-Darias J-A, Ortega Á, Corral-Lugo A, Matilla MA, Krell T. 2016. McpQ is a specific citrate chemoreceptor that responds preferentially to citrate/metal ion complexes. Environ Microbiol 18:3284–3295.
28. Li M, Hazelbauer GL. 2005. Adaptational assistance in clusters of bacterial chemoreceptors. Mol Microbiol 56:1617–26.
29. Matilla MA, Martín-Mora D, Gavira JA, Krell T. 2021. Pseudomonas aeruginosa as a Model To Study Chemosensory Pathway Signaling. Microbiol Mol Biol Rev 85:e00151-20.
30. Ortega DR, Fleetwood AD, Krell T, Harwood CS, Jensen GJ, Zhulin IB. 2017. Assigning chemoreceptors to chemosensory pathways in Pseudomonas aeruginosa. Proc Natl Acad Sci USA 114:12809–12814.
31. García-Fontana C, Corral Lugo A, Krell T. 2014. Specificity of the CheR2 methyltransferase in Pseudomonas aeruginosa is directed by a C-terminal pentapeptide in the McpB chemoreceptor. Sci Signal 7:ra34.
32. Djordjevic S, Stock AM. 1998. Chemotaxis receptor recognition by protein methyltransferase CheR. Nat Struct Biol 5:446–50.
33. Shiomi D, Okumura H, Homma M, Kawagishi I. 2000. The aspartate chemoreceptor Tar is effectively methylated by binding to the methyltransferase mainly through hydrophobic interaction. Mol Microbiol 36:132–40.
34. Lai W-C, Barnakova LA, Barnakov AN, Hazelbauer GL. 2006. Similarities and differences in interactions of the activity-enhancing chemoreceptor pentapeptide with the two enzymes of adaptational modification. J Bacteriol 188:5646–5649.
35. Mansfield J, Genin S, Magori S, Citovsky V, Sriariyanum M, Ronald P, Dow M, Verdier V, Beer SV, Machado MA, Toth I, Salmond G, Foster GD. 2012. Top 10 plant pathogenic bacteria in molecular plant pathology. Mol Plant Pathol 13:614–29.

36. Toth IK, Bell KS, Holeva MC, Birch PR. 2003. Soft rot erwiniae: from genes to genomes. Mol Plant Pathol 4:17–30.
37. Matilla MA, Velando F, Tajuelo A, Martín-Mora D, Xu W, Sourjik V, Gavira JA, Krell T. 2022. Chemotaxis of the Human Pathogen Pseudomonas aeruginosa to the Neurotransmitter Acetylcholine. mBio 13:e0345821.
38. Velando F, Matilla MA, Zhulin IB, Krell T. 2023. Three unrelated chemoreceptors provide Pectobacterium atrosepticum with a broad-spectrum amino acid sensing capability. Microb Biotechnol 16:1548–1560.
39. Monteagudo-Cascales E, Ortega Á, Velando F, Morel B, Matilla MA, Krell T. 2023. Study of NIT domain-containing chemoreceptors from two global phytopathogens and identification of NIT domains in eukaryotes. Mol Microbiol 119:739–751.
40. Yi X, Weis RM. 2002. The receptor docking segment and S-adenosyl-L-homocysteine bind independently to the methyltransferase of bacterial chemotaxis. Biochim Biophys Acta 1596:28–35.
41. Matilla MA, Velando F, Martín-Mora D, Monteagudo-Cascales E, Krell T. 2022. A catalogue of signal molecules that interact with sensor kinases, chemoreceptors and transcriptional regulators. FEMS Microbiol Rev 46:fuab043.
42. Feng X, Lilly AA, Hazelbauer GL. 1999. Enhanced function conferred on low-abundance chemoreceptor Trg by a methyltransferase-docking site. J Bacteriol 181:3164–71.
43. Lai W-C, Hazelbauer GL. 2005. Carboxyl-terminal extensions beyond the conserved pentapeptide reduce rates of chemoreceptor adaptational modification. J Bacteriol 187:5115–5121.
44. Reyes-Darias JA, Yang Y, Sourjik V, Krell T. 2015. Correlation between signal input and output in PctA and PctB amino acid chemoreceptor of Pseudomonas aeruginosa. Mol Microbiol 96:513–525.
45. Feng X, Baumgartner JW, Hazelbauer GL. 1997. High- and low-abundance chemoreceptors in Escherichia coli: differential activities associated with closely related cytoplasmic domains. J Bacteriol 179:6714–20.
46. Zatakia HM, Arapov TD, Meier VM, Scharf BE. 2018. Cellular Stoichiometry of Methyl-Accepting Chemotaxis Proteins in Sinorhizobium meliloti. J Bacteriol 200:e00614-17.

47. Hazelbauer GL, Engström P. 1980. Parallel pathways for transduction of chemotactic signals in Escherichia coli. Nature 283:98–100.
48. Akkaladevi N, Bunyak F, Stalla D, White TA, Hazelbauer GL. 2018. Flexible Hinges in Bacterial Chemoreceptors. J Bacteriol 200:e00593-17.
49. Sambrook J, Fritsch EF, Maniatis T. 1989. Molecular Cloning: A Laboratory Manual, 2nd edn. Cold Spring Harbor Laboratory Press, New York, NY, USA.
50. Li M, Hazelbauer GL. 2004. Cellular stoichiometry of the components of the chemotaxis signaling complex. J Bacteriol 186:3687–94.
51. Anderson, T.F. Techniques for the preservation of three-dimensional structure in preparing specimens for the electron microscope. Trans N Y Acad Sci 13:130–134.
52. Trueba FJ, Woldringh CL. 1980. Changes in cell diameter during the division cycle of Escherichia coli. J Bacteriol 142:869–878.
53. Jumper J, Evans R, Pritzel A, Green T, Figurnov M, Ronneberger O, Tunyasuvunakool K, Bates R, Žídek A, Potapenko A, Bridgland A, Meyer C, Kohl SAA, Ballard AJ, Cowie A, Romera-Paredes B, Nikolov S, Jain R, Adler J, Back T, Petersen S, Reiman D, Clancy E, Zielinski M, Steinegger M, Pacholska M, Berghammer T, Bodenstein S, Silver D, Vinyals O, Senior AW, Kavukcuoglu K, Kohli P, Hassabis D. 2021. Highly accurate protein structure prediction with AlphaFold. Nature, 2021/07/16 ed. 596:583–589.
54. Schrodinger L. 2010. The PyMOL Molecular Graphics System, Version 1.3r1. New York: Schro¨ dinger, LLC.

Fig. 1

A

```
ECA_RS00895   …LADAVSAFKIPSYSHGNAGSYESVPMSTPTLSLALARKE
ECA_RS00900   …LAEAVSTFKLLSYGNGKTASYASAPTRTPTLSLAPAAAKNQSNNDNWTTF
ECA_RS08780   …LARTVSVFNLGASYKSAALNRKTETPALAAPKNNRAEKTSAKGELADWTTF
ECA_RS10160   …LSHAVAAFRI
ECA_RS18000   …LAETVSQFRLGNGHQIARTPAAAASLTLRPALAAPGKSGISAGEGDWTSF
ECA_RS21440   …LVELMKVFIVEGGSSQRIAPPLKRPSSAKFSLANPKGSAGSNNQNWEQF
ECA_RS21445   …LVELMKVFIVESGSSQRTTPELKRPSSAKLSLASPKGRTKSDSQNWETF
ECA_RS20365   …LVTLMNHFHLRGTPAARPAPMAKKAQTARLALAPVGNTQDNWEKF
ECA_RS21450   …LLELMGVFKLNGIQTKAPRLTSQVKQPAAPRLALASKSGHTSSDNWETF
ECA_RS21455   …LVELMGVFKIDGTQSQRAVPQVTTLSRPKLALAGNSSNTNWETF
ECA_RS12390   …LNEQAQELSRTVEQFRVDESAGSYLALGAR
ECA_RS02220   …LRDAVRFFKVNQDHLLRIH
ECA_RS06345   …LQNAVEVFKINQAVAQEHRAASASSLAALPKSLLPKPTSAGSSNANWETF
ECA_RS08370   …LNQAVAVFRLSEDTGSFRRTTQATAGQKPVLLAPSVNGGKKAKEGSSTDNWETF
ECA_RS08330   …LTRAVATFKLSSHLSSGHSAPARPNALAAKGRSSLALPRQANTENGNWETF
ECA_RS19280   …LTQAVAVFKLSGIVQQVRSSLPKSAPQPRLAPAMAIAGSSKGNSNQNWETF
ECA_RS18955   …LNLGVSRFHLM
ECA_RS06625   …LNQTVSLFQLSDTQSALQVAAKPVRKAQAIAPRAGKALPTSSDNWEKF
ECA_RS07510   …LSAVVDVFNLDSDSDQQTAFSRPAIAAPVHRAVAQSTTPLLSVHGRHGEGWEKF
ECA_RS13300   …LTEAVSVFQLSAAEAPRRPQQRLAEKAPAAQKPMLLAAAGGKKGNANDNWETF
ECA_RS12635   …LESMVANFRLSENEGRKPKANISGLPPQQKYLPPAAKQTQDSGWTTF
ECA_RS12640   …LEKLLEHFRVSQSDNRVASRASSSIPRHTLPKSVSAKAASSESDWTSF
ECA_RS00400   …LATLMSVFRISDKDVARLQGSNTGNPNSGNKATARLPTLASRDNGNDNWTTF
ECA_RS00455   …LKQAVSVFRLANAQHDDTPAGIAFNNQPHRLHAPR
ECA_RS10935   …LAQTIEHFRLEQQHALPHALLR
ECA_RS17750   …LAESMVQFKVQSQEFAAIGRF
ECA_RS17910   …LMRSMALFQVEPRLS
ECA_RS02005   …LQQSVSRFQIARENREMDNVLPGLRQNITLADAR
ECA_RS15955   …LSQLVGQFIVGQIASSSLIPALASVPSGLSAPRLASAKNKNALAQDEAGWQRF
ECA_RS05475   …LNSVVGAFRV
ECA_RS02210   …MESLVSHFKVDDSAPQQPLQHALLSR
ECA_RS09870   …MSEAVSVFSIPR
ECA_RS09875   …MVQAASVFSLSR
ECA_RS17685   …LNSAINVYGS
ECA_RS17860   …LSELVSVFRI
ECA_RS11380   …LNTSVSLFILPSTEADVNPMIDQREMTQRIPMMG
```

B

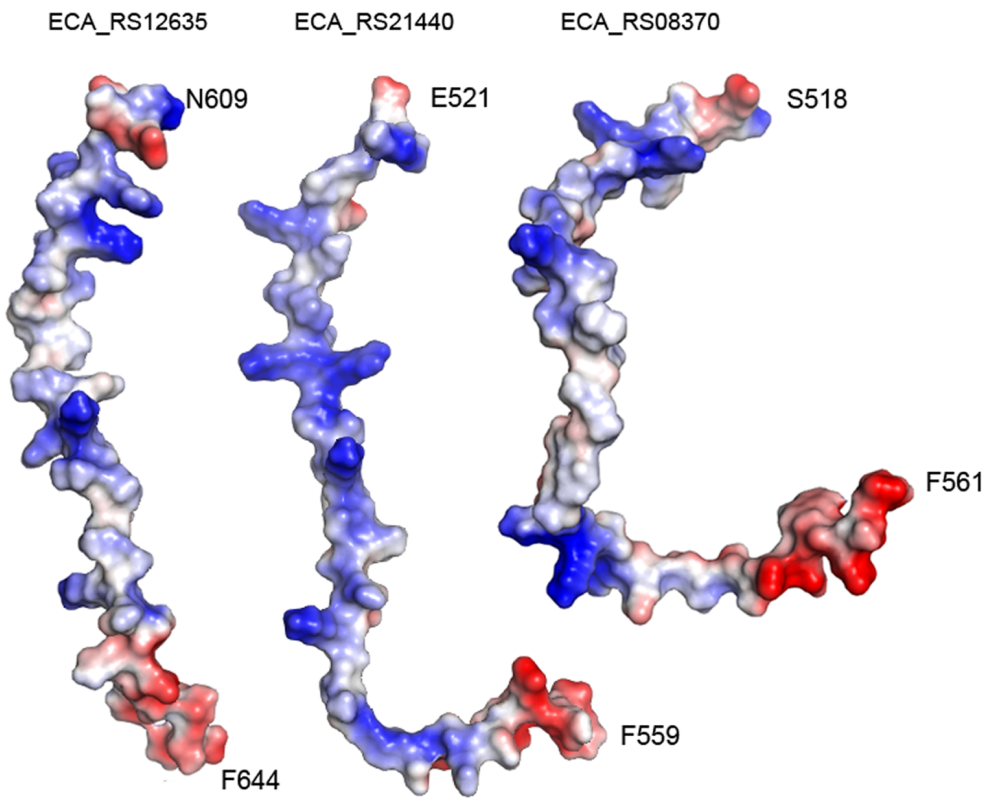

Fig. 2

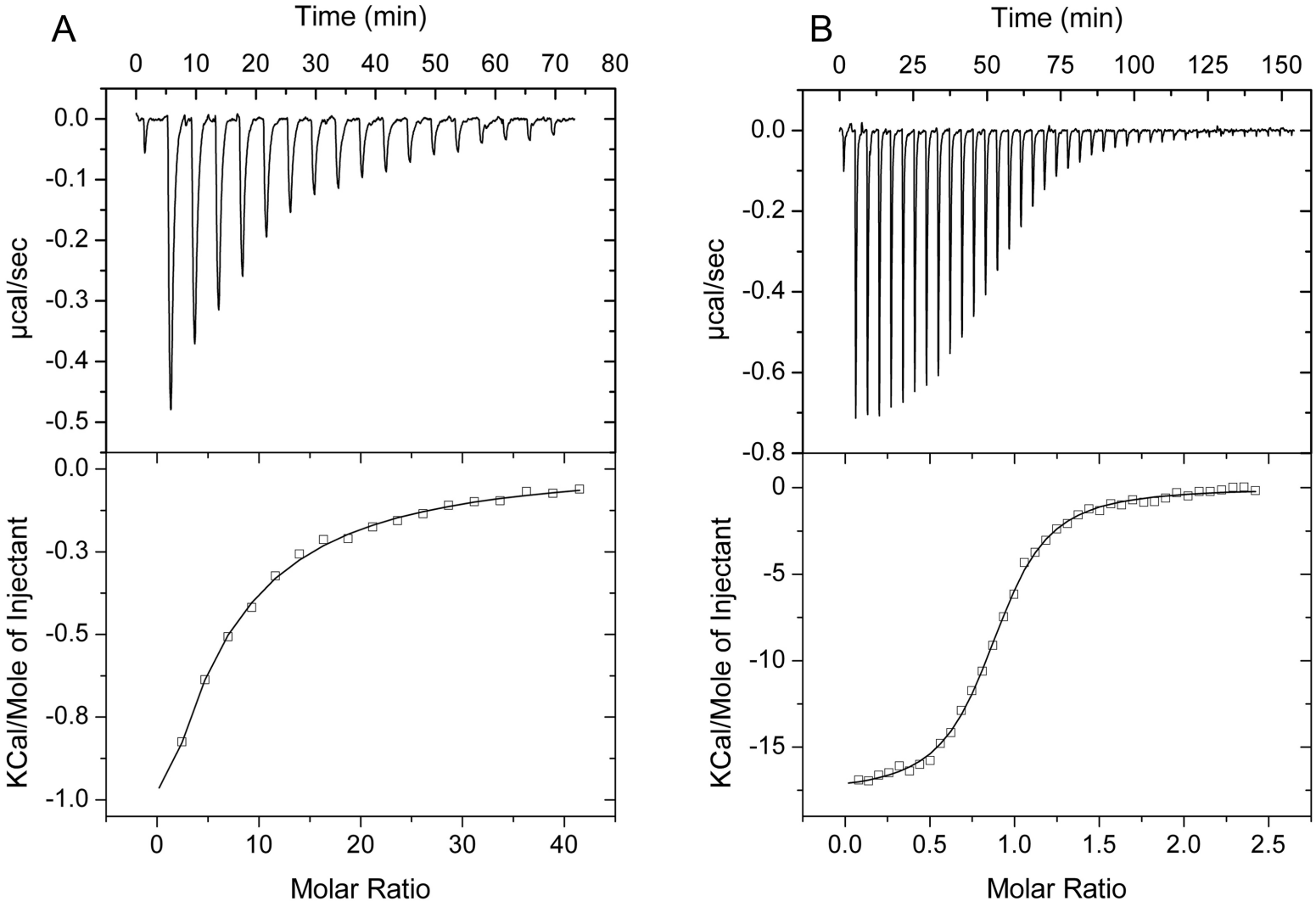
A
Time (min)
0 10 20 30 40 50 60 70 80
0.0 -0.1 -0.2 -0.3 -0.4 -0.5
µcal/sec
0.0 -0.3 -0.5 -0.8 -1.0
KCal/Mole of Injectant
0 10 20 30 40
Molar Ratio
B
Time (min)
0 25 50 75 100 125 150
0.0 -0.2 -0.4 -0.6 -0.8
µcal/sec
0 -5 -10 -15
KCal/Mole of Injectant
0.0 0.5 1.0 1.5 2.0 2.5
Molar Ratio

Fig. 3

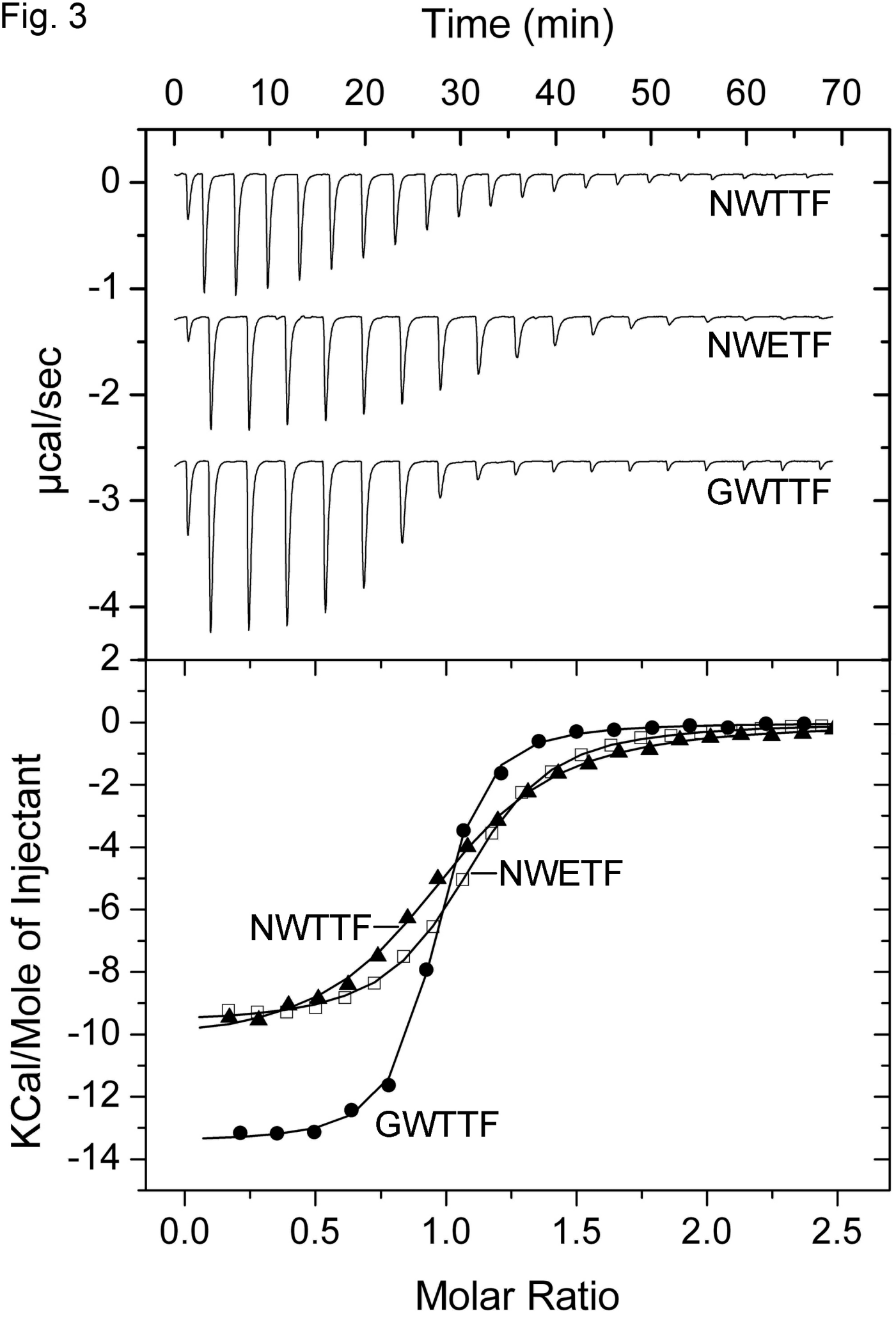
Time (min)
0
10
20
30
40
50
60
70
0
-1
-2
-3
-4
μcal/sec
NWTTF
NWETF
GWTTF
2
0
-2
-4
-6
-8
-10
-12
-14
KCal/Mole of Injectant
NWETF
NWTTF
GWTTF
0.0
0.5
1.0
1.5
2.0
2.5
Molar Ratio

Fig. 4

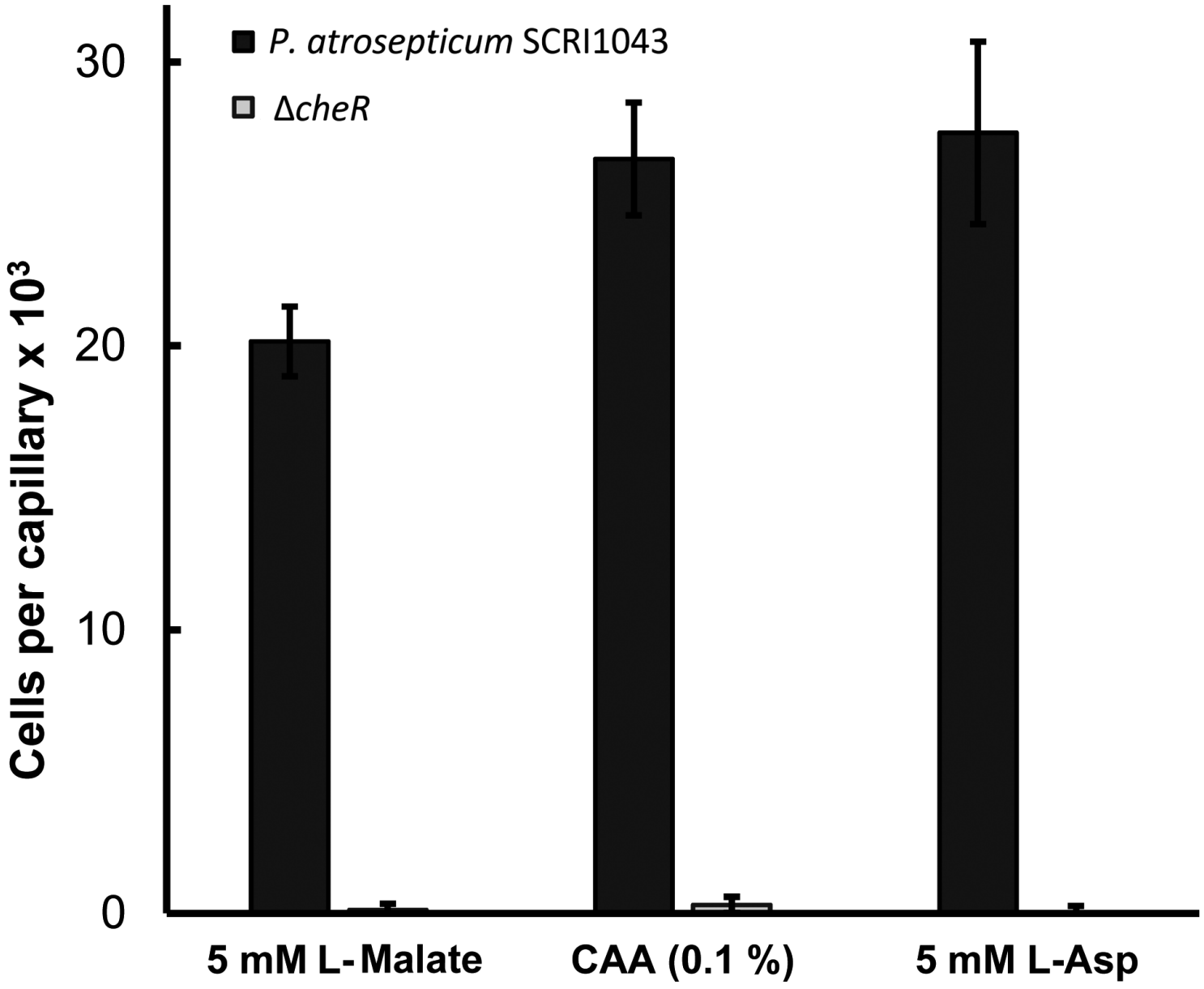
P. atrosepticum SCRI1043
ΔcheR
Cells per capillary x 10³
30
20
10
0
5 mM L-Malate
CAA (0.1 %)
5 mM L-Asp

Fig. 5

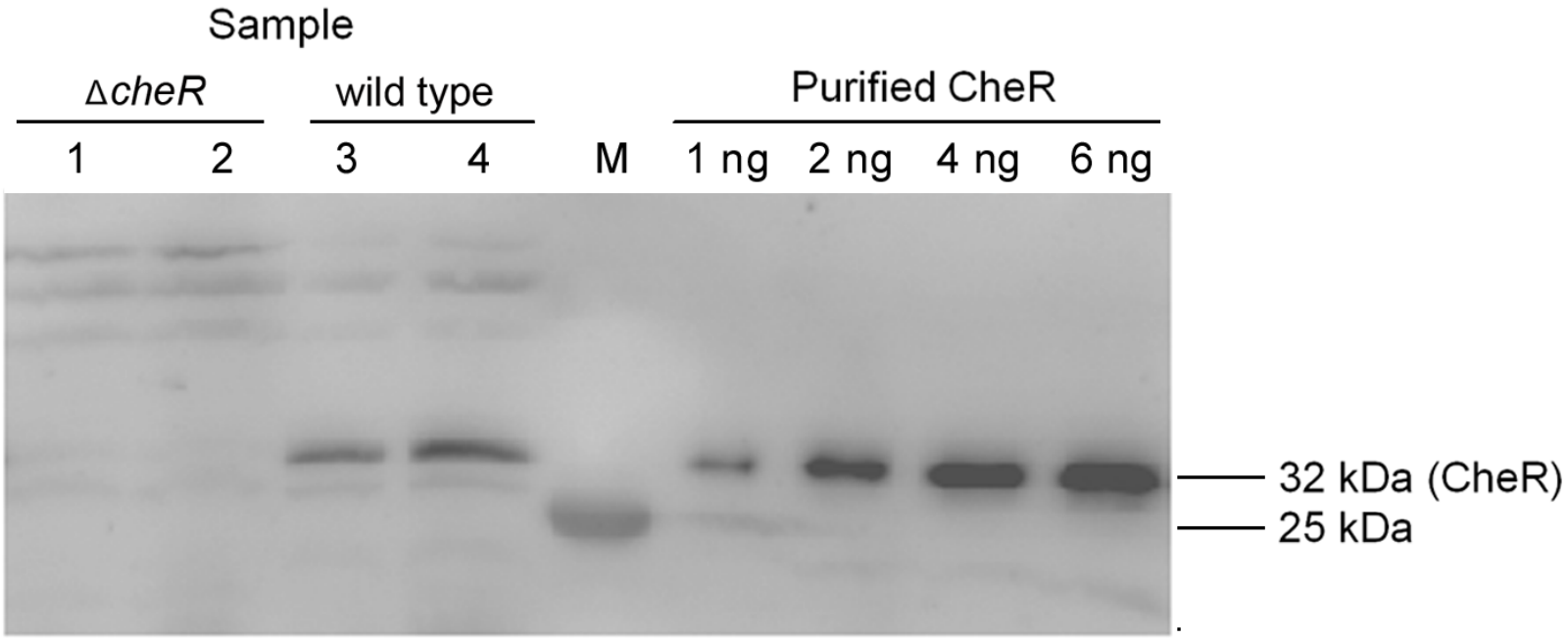
Sample
ΔcheR
wild type
Purified CheR
1
2
3
4
M
1 ng
2 ng
4 ng
6 ng
32 kDa (CheR)
25 kDa

Fig. 6

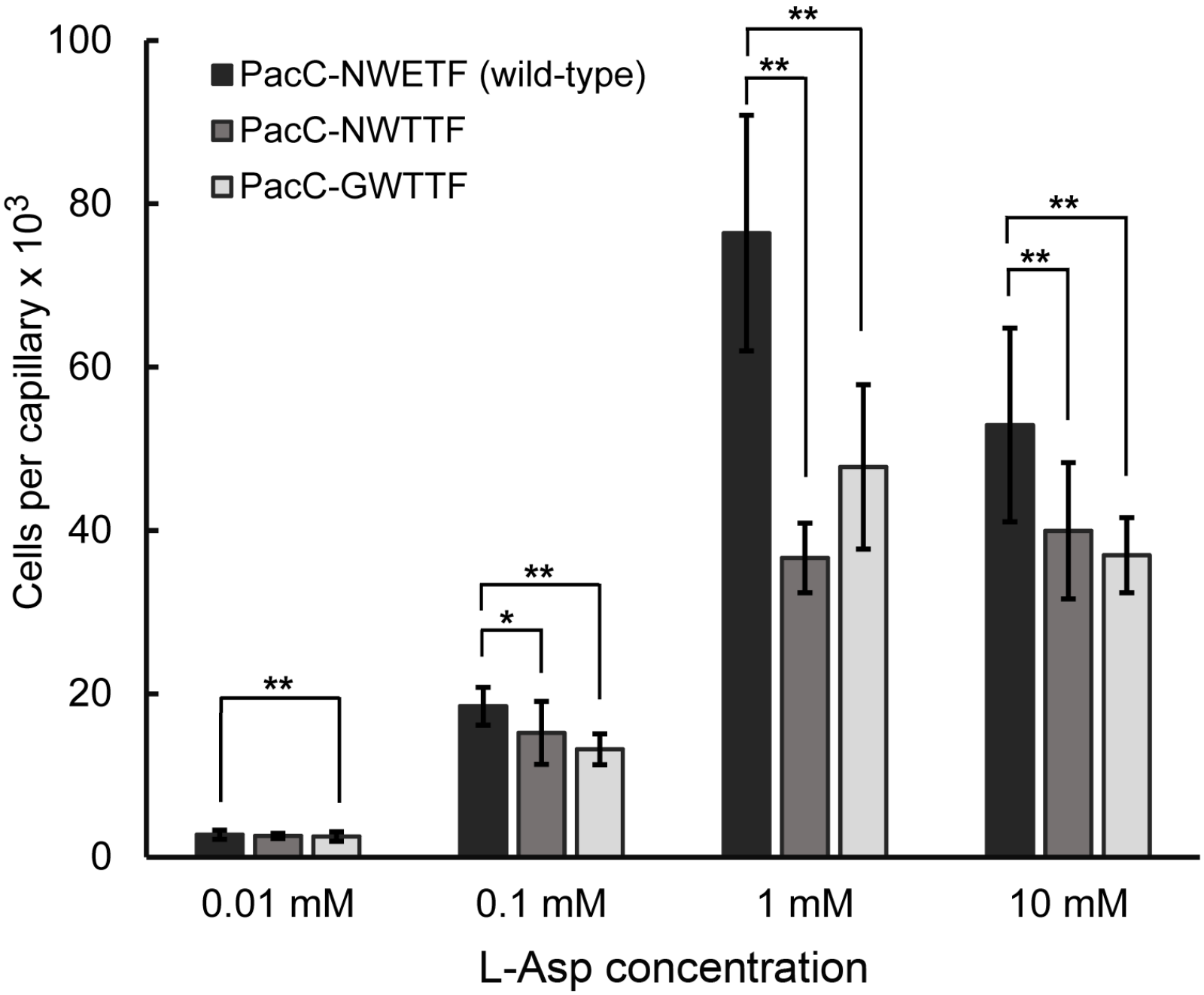
PacC-NWETF (wild-type)
PacC-NWTTF
PacC-GWTTF
Cells per capillary x 10^3
100
80
60
40
20
0
**
*
0.01 mM
0.1 mM
1 mM
10 mM
L-Asp concentration